Gas sensing characteristics of two-dimensional palladium-based penta-materials

J. D. Correa[a], Leonor Chico[b], V. Nuñez[c], S. Bravo[c], M. Pacheco[c]

[a] *Facultad de Ciencias Básicas, Universidad de Medellín, Medellín, Colombia*
[b] *GISC, Departamento de Física de Materiales, Facultad de Ciencias Físicas, Universidad Complutense de Madrid, 28040 Madrid, España*
[c] *Departamento de Física, Universidad Técnica Federico Santa María, Valparaíso, Chile*

Abstract

The experimental discovery of two-dimensional penta-materials $PdSe_2$ and PdPSe has boosted interest in their potential applications. In this work, we present a systematic ab initio study of the electronic properties of penta-$PdSe_2$ and penta-PdPSe as sensors of molecules such as H_2, CO, and NO, which are potentially dangerous gases. We find that Pd-based penta-materials are excellent sensors for NO molecules according to the adsorption energies and recovery times. Most importantly, they present a change from semiconducting to metallic behavior upon NO adsorption which points to their potential application for optoelectronic gas sensors

Keywords: DFT, 2D, Penta, Sensor, NO

1. Introduction

Since the obtention of graphene by Geim and Novoselov [1], the experimental and theoretical characterization of two-dimensional (2D) materials is a tremendously active research topic due to diverse reasons; among them, the great number of potential applications, the emergence of new physical phenomena and, very importantly, the easiness to tune their properties as compared to their bulk counterparts [2, 3, 4, 5, 6, 7, 8, 9, 10]. These 2D materials can be obtained by top-down approaches, such as liquid or mechanical exfoliation of 3D layered crystals, or bottom-up techniques, such as molecular beam epitaxy (MBE), chemical vapor deposition (CVD), and physical vapor deposition (PVD)

among other methods. Their composition is quite varied; some of the most studied 2D materials are transition metal chalcogenides, hexagonal boron nitride (h-BN), boron phosphide (BP), phosphorene, silicene, germanene, and a long list that increases from year to year [11, 12]. Motivated by a large number of synthesized and theoretically proposed 2D materials, computational 2D materials databases (C2DMDB) arise as alternatives to classify the stability and their basic physicochemical properties [2, 4, 5]. The C2DMDB contain several not-yet-synthesized materials that are either theoretically proposed for the first time or that have been put forward previously and have been verified to be thermally and dynamically stable. One example of this is penta-graphene (PG), a new allotrope of carbon composed by pentagons. Penta-graphene was first proposed in 2014 by Tang *et al.* [13] and later by Zhang *et al.* [14]. Although PG has not been synthesized so far, its physicochemical properties have been widely explored through first-principles calculations, showing its possibilities as gas sensors, the development of Li-ion batteries and other new optoelectronic devices [15, 16, 17, 18, 19].

Due to the excellent possibilities of PG for the development of new devices as well as its interesting basic properties, which stimulates the exploration of fundamental physical phenomena, other pentagonal structures based on a combination of different atomic species have been explored. Standing out, penta-silicene [20], a family of X_2C, with X = (P, As, Sb)[21], a binary family of MX_2 with (M=Ni, Pd, Pt; X=P, As), Pt_2N_4 [22], pentagonal transition-metal (group X) chalcogenide monolayers [23], and the palladium family of pentamaterials, penta-$PdSe_2$ and penta-PdPSe, recently obtained by mechanical exfoliation of crystal bulk [24, 25]. Palladium diselenide ($PdSe_2$) is a 2D-pentagonal layered noble transition-metal dichalcogenide with a puckered morphology that is stable in air and exhibits a widely tunable bandgap that varies from zero (metallic bulk) to ~ 1.3 eV (semiconductor monolayer) [24]. Atomically thin penta-PdPSe has an orthorhombic structure and belongs to space group no. 60. It is composed of two pentagonal layers with a separation of 0.7 Å coupled by comparatively weak van der Waals interactions. The bandgap of penta-PdPSe varies from 1.46 eV in bulk to 1.92 eV for thinner penta-PdPSe

samples [25].

Penta-materials have potential applications in the development of new sensors for harmful gases. Recently, it has been shown via first-principles calculations that penta-PdPS and penta-PdPSe are suitable candidates for NO and NO_2 sensors [26]. Also, theoretical studies show that penta-$PdSe_2$ is an excellent option to develop water-splitting applications [27].

Motivated by the possibilities of penta-materials in gas sensor applications, we have performed a systematic study of the electronic properties of penta-$PdSe_2$ and penta-PdPSe as sensors of small hazardous molecules, such as H_2, CO, CO_2 and NO. Adsorption energies, recovery times, and changes induced by the adsorption of the molecules on the optoelectronic properties of the penta-$PdSe_2$ and penta-PdPSe are computed by means of first-principles calculations. We verify the validity and robustness of our results by using several exchange-correlation functionals, including van der Waals interactions.

2. Computational Methodology

We employ a first-principles methodology in the the framework of density functional theory (DFT), as implemented in GPAW [28, 29] and SIESTA [30] packages. For the basis set on GPAW we employed a plane wave with an energy cutoff of 650 eV. In SIESTA we employed a linear combination of atomic orbitals (LCAO) with a double -ζ polarized basis set. For the k-points, we used a grid of $15 \times 15 \times 1$ for the unit cell and $7 \times 7 \times 1$ for the supercell $2 \times 2 \times 1$. All structures are fully relaxed until the atomic forces in each atom were less than 0.02 eV/Å. For the exchange-correlation functional we used several approaches of the GGA family, namely, PBE [31], RPBE [32], and revPBE [33]. In order to include the van der Waals (vdW) interaction we employed the vdW-DF [34], vdW-DF2 [34], and optB88-vdW [35] functionals.

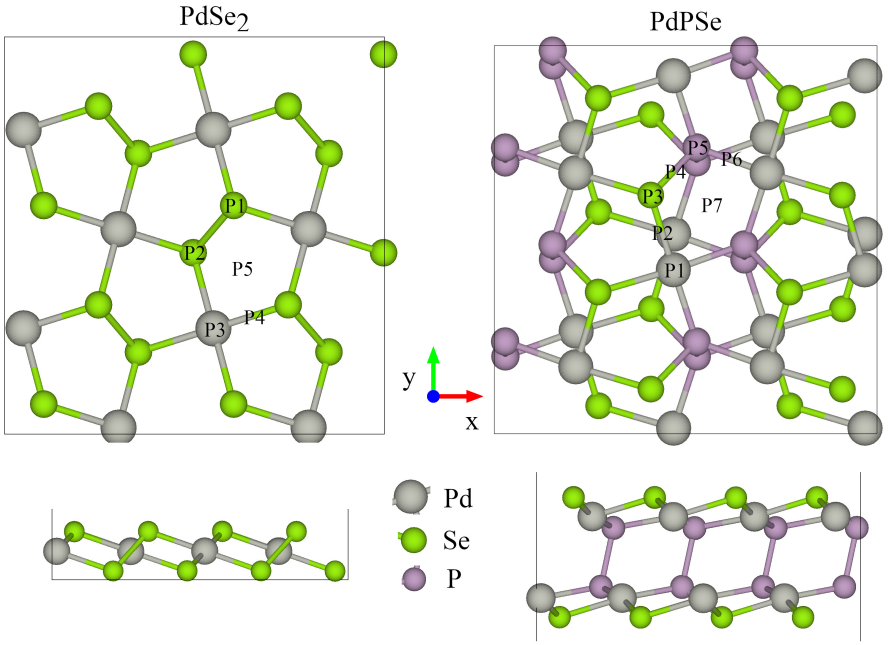

Figure 1: Schematic representation of the relaxed geometry of penta-$PdSe_2$ and penta-PdPSe. The results are obtained with the GPAW code employing the PBE exchange-correlation functional. The PX labels indicate the initial adsorption position considered for molecules on penta-$PdSe_2$ and penta-PdPSe.

3. Results

3.1. Geometric Structure

The penta-$PdSe_2$ monolayer can be viewed as three atomic layers tightly bonded. The central layer of the structure is composed of Pd atoms, situated between two layers of Se atoms. This structure confers a buckled geometry to the penta-$PdSe_2$ layer, as it is shown in Fig. 1. The values of the lattice constants and the bandgap of penta-$PdSe_2$ are reported in Table 1. Comparing the results for the lattice constants of bulk $PdSe_2$ computed with different exchange-correlation functionals with the experimental values reported in [24], we observe that the PBE functional shows the largest difference, 0.05Å, for the b lattice parameter. When vdW interactions are considered, the maximum difference in the lattice constant is 0.26 Å, obtained for the vdW-DF2 functional. This agrees with a previous report of theoretical lattice parameters of bulk-$PdSe_2$.

penta-$PdSe_2$

Exchange-correlation	a(Å)	b(Å)	gap(eV)
PBE	5.74694	5.91884	1.338
LDA	5.60078	5.78370	1.444
RPBE	5.81061	5.97571	1.256
revPBE	5.79413	5.96133	1.281
vdW-DF	5.85769	6.05296	1.169
vdW-DF2	5.93773	6.12769	1.080
optPBE-vdW	5.7785	5.98201	1.269
SIESTA	5.7995	6.05096	1.211
C09-vdW	5.65705	5.87521	1.420
GLLBSC			2.050
exp-bulk [24]	5.7457	5.8679	

penta-PdPSe

Exchange-correlation	a(Å)	b(Å)	gap(eV)
PBE	5.84960	5.90720	1.108
LDA	5.73997	5.78863	1.171
RPBE	5.89355	5.95226	1.086
revPBE	5.88490	5.93966	1.094
vdW-DF	5.96822	6.04448	0.934
vdW-DF2	6.03519	6.03519	0.850
optPBE-vdW	5.90887	5.98340	0.976
SIESTA	6.00955	6.08469	0.693
C09-vdW	5.82330	5.89056	1.025
GLLBSC			1.880
exp-bulk [36]	5.7457	5.8679	

Table 1: Lattice parameters and energy band gap for penta-$PdSe_2$ and penta-PdPSe. Several exchange-correlation functionals are considered. All results are obtained with the GPAW code.

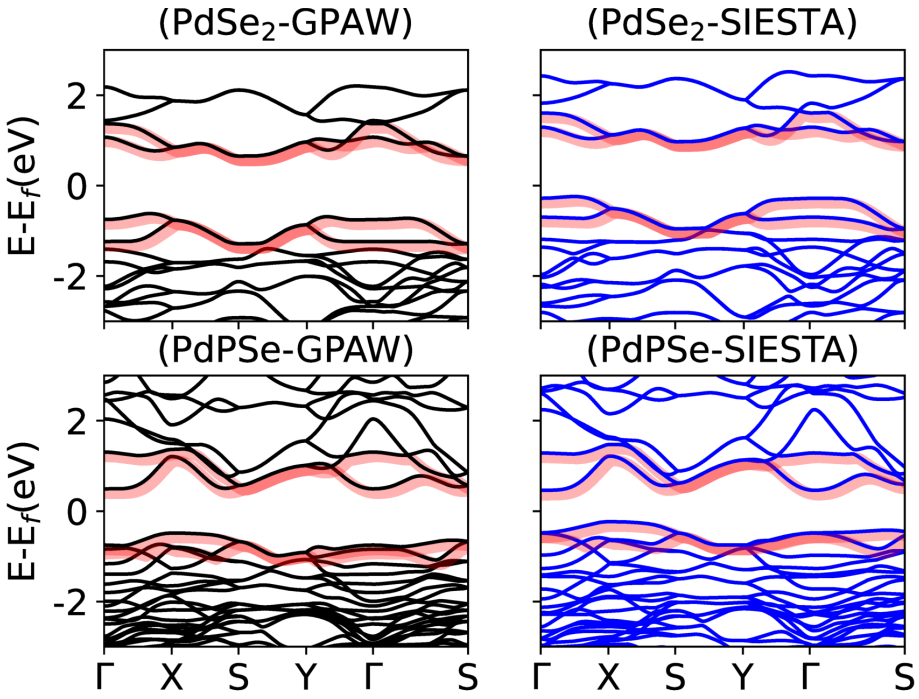

Figure 2: Band structures of penta-$PdSe_2$ and penta-PdPSe monolayers obtained with SIESTA-optB88-vdW and GPAW-optB-vdW. The lowest conduction bands and highest valence bands are highlighted in red to emphasize their similarity, showing that both methods give equivalent results for the relevant bands in optical calculations.

Analogously, the penta-PdPSe monolayer can be considered as being composed of two layers, which are covalently bonded via the P atom in each layer. Each one of these two layers is in turn composed of three atomic layers, with a central Pd layer between two layers of P and Se atoms, as it is shown in Fig. 1. The values of the lattice constants and the bandgap of penta-PdPSe are reported in Table 1. As for $PdSe_2$, a comparison of the numerical results obtained with different exchange-correlation functionals to the reported experimental lattice constants for bulk-PdPSe, yields a maximum difference of 0.05Å for the b lattice parameter with the PBE functional. If vdW interactions are considered, the maximum difference in the lattice constant is 0.26Å for the vdW-DF2 functional. This is in agreement with a previous report of theoretical lattice parameters of bulk-PdPSe [36]. In general, vdW functionals overestimate the lattice parameters with respect to the GGA approximation. This behavior is usual in vdW exchange-correlation

functionals, as previously reported [25].

The geometric parameters of the penta-$PdSe_2$ and penta-PdPSe obtained with the SIESTA code for the optB88-vdW exchange-correlation functional are similar to those obtained with GPAW, particularly for PBE and optPBE-vdW. This suggests that different exchange-correlation functionals along with various representations of the Kohn-Sham states are equally adequate to study the electronic structure of penta-Pd families, showing the robustness of our results. Therefore, we study the adsorption of small molecules onto penta-$PdSe_2$ and penta-PdPSe surfaces with the SIESTA code employing the optB88-vdW exchange-correlation functional, since SIESTA has a cheaper computational cost than plane wave codes such as GPAW. Additionally, in Fig. 2 we show the band structures of penta-$PdSe_2$ and penta-PdPSe monolayers obtained with GPAW and SIESTA. Red shadows highlight the valence and conduction bands closest to the Fermi level. This zone is the most relevant for the calculation of optical properties, such as the dielectric function and their derivatives, i.e., macroscopic response functions. Therefore, similarly to what we found with respect to the geometric parameters, we corroborate that the electronic band structures are equally well described by GPAW and SIESTA, thus supporting the election of SIESTA to obtain the optoelectronic properties of the adsorption of small molecules onto penta-Pd families on the basis of its lower computational cost.

3.2. Adsorption of molecules

The adsorption of H_2, CO, and NO on penta-Pd families is studied considering several initial positions, as shown in Fig. 1, and labeled as PX, where X is a number. For penta-$PdSe_2$, we considered five of such positions: P1 and P2 are at the top of Se atoms, P3 is at the top of the Pd atom, P4 is in the Pd-Se bridge, and P5 is in the pentagonal hollow site. For penta-PdPSe, seven positions are considered: P1 is at the top of Pd, P2 is in the Pd-Se bridge, P3 is at the top of Se, P4 is in the P-Se bridge, P5 is at the top of the P atom, P6 is in the Pd-P bridge, and P7 is in the pentagonal hollow site. In the Supplementary Material, Fig-S1 and Fig-S2 show all the final relaxed positions for the NO molecule onto penta-$PdSe_2$ and penta-PdPSe.

	H_2			CO			NO		
Position	E_a(meV)	ΔQ	d(Å)	E_a(meV)	ΔQ	d(Å)	E_a(meV)	ΔQ	d(Å)
				penta-$PdSe_2$					
P1	-39.4	0.008	3.185	-54.2	0.034	2.536	-181	0.020	2.308
P2	-49.0	0.018	1.985	-69.1	0.036	2.057	-285	0.055	1.475
P3	-58.6	0.026	1.714	-22.7	0.097	1.776	-263	0.075	1.812
P4	-38.9	0.014	2.462	-71.9	0.025	2.458	-202	0.052	2.028
P5	-45.7	0.013	2.534	-66.4	0.029	2.329	-354	0.041	1.817
				penta-PdPSe					
P1	-56.2	0.024	1.838	-169	0.066	1.918	-516	0.056	1.505
P2	-49.8	0.146	2.417	-156	0.065	1.987	-238	-0.009	1.989
P3	-42.2	0.008	3.313	-64	0.030	2.813	-310	0.003	2.042
P4	-55.2	0.008	2.639	-77	0.030	2.092	-298	0.006	1.774
P5	-49.1	0.022	1.904	-100	0.04	2.103	-297	-0.007	1.572
P6	-49.6	0.021	1.932	-173	0.05	2.007	-393	0.007	1.509
P7	-54.6	0.021	1.764	-81	0.029	2.038	-538	0.043	1.273

Table 2: Values of the adsorption energy (E_a), charge transfer (ΔQ), and minimal distance between molecule and penta-material (d). Three molecules are considered, namely, H_2, CO, and NO. The adsorption surfaces are penta-$PdSe_2$ and penta-PdPSe.

In order to identify the most likely absorption site, we calculate the adsorption energy, given by

$$E_a = E_{penta+mol} - (E_{penta} + E_{mol}), \tag{1}$$

where $E_{penta+mol}$ is the energy of the penta-material plus the adsorbed molecule, E_{penta} is the energy of the pristine 2D penta-material, and E_{mol} is the energy of the isolated molecule. The adsorption energies are shown in Table 2 for all the molecules considered in this work. Starting with H_2, the largest adsorption energy for both penta-monolayers occurs at the top of the Pd atom; however, the obtained values, -58.6 meV for penta-$PdSe_2$ and -56.2 meV for penta-PdPSe, are low for sensing or storage of hydrogen molecules: Note that for storage applications, the adsorption energy of a single molecule must be in the range of 0.2 to 0.6 eV [37].

These values contrast with that reported in previous work for pristine pentagraphene,

which indicates adsorption energy of -92 meV, that could be increased by doping the system with transition-metal atoms [38]. It is also at variance with previous studies in which Pd atoms are used for decorating nanomaterials with the aim to increase their H_2 adsorption capacity [39, 40, 41]. These comparisons suggest that the efficiency of Pd atoms to adsorb H_2 molecules depends on the chemical environment.

With respect to the CO molecule, both pentamaterials show significant adsorption energy in the Pd-Se bridge if the molecule is oriented with the C atom pointing to the surface. The adsorption energies are larger than those obtained for the H_2 molecule. Notwithstanding, our maximal adsorption energy is -175 meV, smaller than the reported value for PG, being -520 meV [42]. These results indicate that Pd atoms do not constitute a favorable chemical environment for the adsorption of CO molecules, based on the comparison to pentagraphene without any adsorbed metals.

Remarkably, the adsorption of NO molecules contrasts with that of H_2 and CO molecules: NO on penta-Pd families shows an adsorption energy higher than on pentagraphene and other 2D-materials [43]. In this case, the adsorption energy is maximum for the hollow position of both penta-Pd materials, being the largest for penta-PdPSe with a value of -538 meV. These results are in concordance with a previous report that suggests that penta-PdPSe and penta-PdPS are excellent candidates for adsorption of NO [26]. However, the adsorption energy we find in our calculation is around half the value reported previously, in which they employed the Grimme correction DFT-D3 [44].

Likewise, three different orientations of the molecules were considered: perpendicular to the surface with the O atom pointing to the surface, perpendicular to the surface with the C/N atom pointing to the surface, and parallel to the surface. We find that the oxygen atom experiments a repulsion by the surface, so the adsorption with the oxygen atom pointing to the surface is the configuration with the lowest adsorption energy (-57 meV for NO onto penta-$PdSe_2$ in position P5, and -92 meV for NO onto penta-PdPSe in position P7). Due to this repulsion, when the NO molecule is placed parallel to the penta-$PdSe_2$ surface, it undergoes a reorientation, reaching the same configuration as

that obtained when the molecule is placed perpendicularly to the surface with the N atom pointing towards it. However, if the NO molecule is set parallel to the penta-PdPSe surface, it keeps this configuration, but with an adsorption energy of -208 meV. This suggests that the preferred configuration for the molecules is effectively vertical, with the C or N atoms pointing at the surface. An example illustrating these results is included in the supplementary material, Fig-S3.

The recovery time is an important parameter for gas sensing analysis and depends dramatically on the the adsorption energy. Using the transition state theory, they are related by the following expression [45]:

$$\tau = A^{-1} e^{-\frac{E_a}{k_B T}}, \tag{2}$$

where A is the attempt frequency, taken as 10^{12}s^{-1}; k_B is the Boltzmann constant, and T is the temperature. With these values, we find the following recovery times: For H_2 on penta-$PdSe_2$ is 9.7×10^{-12} s, while on penta-PdPSe is 8.8×10^{-12} s. For CO, the recovery times found are 1.5×10^{-11}s and 8.1×10^{-10}s for penta-$PdSe_2$ and penta-PdPSe, respectively. Finally, for NO adsorption, we obtained 8.8×10^{-7}s for penta-$PdSe_2$ and 1.1×10^{-3}s for penta-PdPSe. These values suggest that NO is the best molecule to be sensed in the penta-Pd materials studied, with the largest recovery times – recall that small values of recovery time indicate that it is impossible to sense the molecule before its desorption occurs. Therefore, in spite of the numerical difference in the energy adsorptions reported here and those presented in Ref. [44], we agree on the suitability of these materials for NO detection.

Another important aspect of molecule adsorption is the type of the interaction occurring between the molecules and the surface, and whether the bonding is of physical or chemical character. This has been previously studied for multiple systems employing the deformation electron densities or the electronic localization function (ELF) [46, 47]. Fig. 3 displays the ELF for each NO molecule in the position of maximal adsorption

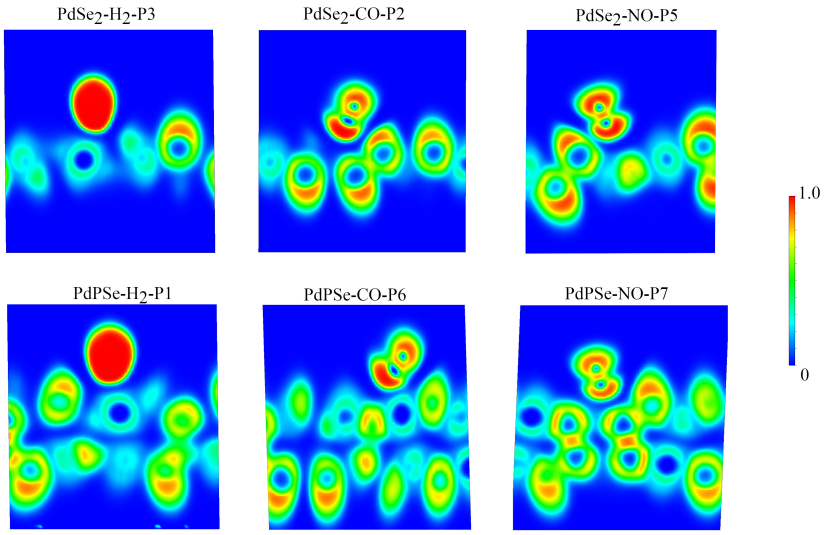

Figure 3: ELF for H_2, CO, and NO molecules adsorbed at the highest energy position on both penta-PdSe2 and penta-PdPSe. The plane used to plot the ELF is the one that connects the molecule axis with the surface atom closest to the molecule.

energy for the penta-PdPSe and penta-$PdSe_2$ surfaces. The ELF is an accepted method to determine the formation of covalent bonds in molecules and solids, independent of the theory level used [48]. If the ELF is near 1, the atoms form covalent bonds; if it is around 0.5, the atoms form ionic bonds. In our case, the ELF between the atoms and the surface is near 0, suggesting a physical bonding between the molecules and the surface, which favors the adsorption-desorption process essential in a sensor.

3.3. Effects on electronic structure

The effects on the electronic structure of the surface due to the adsorption of the molecules are other crucial features to define the sensing behavior of one surface. In this case, we studied the modification of the electronic structure via the total density of states (DOS). For both penta-materials the NO molecules produce the most important change in the electronic structure: the NO molecule changes the behavior of penta-$PdSe_2$ and penta-PdPSe from semiconductor to conductor, showing Van Hove singularities (VHS) just in the Fermi level. There are additionally other VHS in the conduction bands,

with a localization depending on the molecule position, as it is observed in Fig. 4. In contrast, for H_2 and CO molecules penta-$PdSe_2$ and penta-PdPSe surfaces conserve their semiconductor nature. Nonetheless, the minimum of the conduction band and the maximum of the valence band are shifted depending on the position of the molecule, that we attribute to the difference in the charge transfer in each adsorbed position (see Fig-S4 and Fig-S5 in the Supplementary Material).

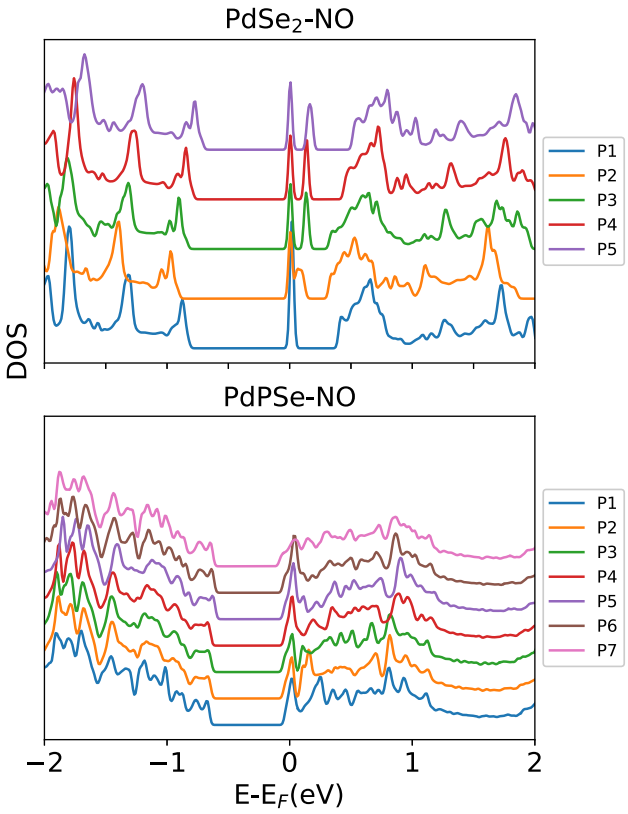

Figure 4: Total density of states for NO molecules adsorbed on penta-$PdSe_2$ and penta-PdPSe. The blue line in each panel represents the DOS of pristine penta-$PdSe_2$ and penta-PdPSe, respectively.

To test the effect of the adsorption molecules onto penta-Pd surfaces, we calculate the optical response of the system via the imaginary part of the dielectric function and the changes induced in the refractive index. We focus on the NO molecule since it shows the most significant changes in the electronic structure of the penta-Pd surfaces. The

imaginary part of the dielectric function for both penta-Pd are shown in Figs. 5 and 6 for two linear polarizations. The polarization directions x and y are specified in Fig. 1. The surface changes from semiconductor to metallic, as observed in the DOS, is the reason for the multiple transitions in the infrared region observed, along with the differences in the optical response around a photon energy of 2 eV. The details of the shape of the spectrum in the infrared region and around 2 eV depending on the adsorption position of the NO molecule. These changes cause a modification in the refractive index and the other optical response functions that can be quantified. A zoom of these specific regions is shown in the Supplementary Material.

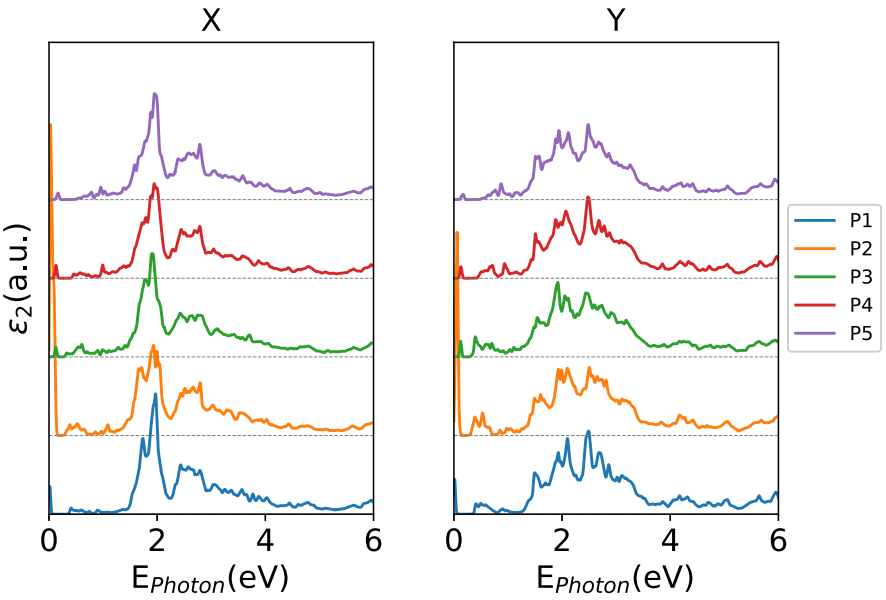

Figure 5: Imaginary part of the dielectric function as a function of the photon energy for the NO molecule onto penta-$PdSe_2$. Several positions of the molecule over the surface are considered and labeled as PX. Two linear polarizations of the incident light are taken into account, namely, along x and y.

3.4. Effects of the concentration of NO molecules

The effects of increasing the concentration of NO molecules on penta-Pd surfaces are also examined. For this purpose, we choose for both surfaces the most probable adsorption position, defined by the adsorption energy. Therefore, for both, penta-$PdSe_2$

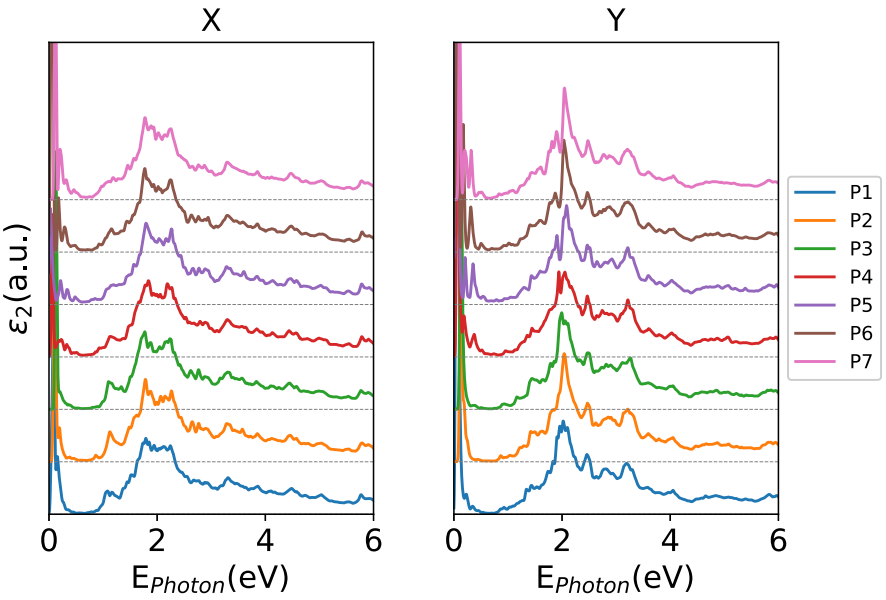

Figure 6: Imaginary part of the dielectric function as a function of the photon energy for the NO molecule onto penta-PdPSe. Several positions of the molecule over the surface are considered and labeled as PX. Two linear polarizations of the incident light are taken into account, namely, along x and y.

and penta-PdPSe, we considered the hole position (P5 and P7, respectively). In these locations, we randomly put from one to five molecules in the supercell chosen for this work (see Sec. 2) and then perform a full relaxation of the system. The electronic structure is re-evaluated via the total density of states. In Fig. 7 the DOS for both penta-Pd with different concentrations of the NO molecules is shown. For all concentrations considered, both materials change from semiconducting to a metallic behavior. Additionally, VHSs close to Fermi level in conduction states are present on both surfaces, and their number and structure increase as NO concentration increases. These results also indicate a more intense interaction between the surface and the adsorbed molecule.

The linear optical response is analyzed to evaluate the change in the physical properties induced by the adsorption of NO molecules and by the increase of the concentration. The dielectric function (real and imaginary parts) is present in Figs. 8 and 9 for two linear polarizations of the incident light (x and y). The results show that the dielectric

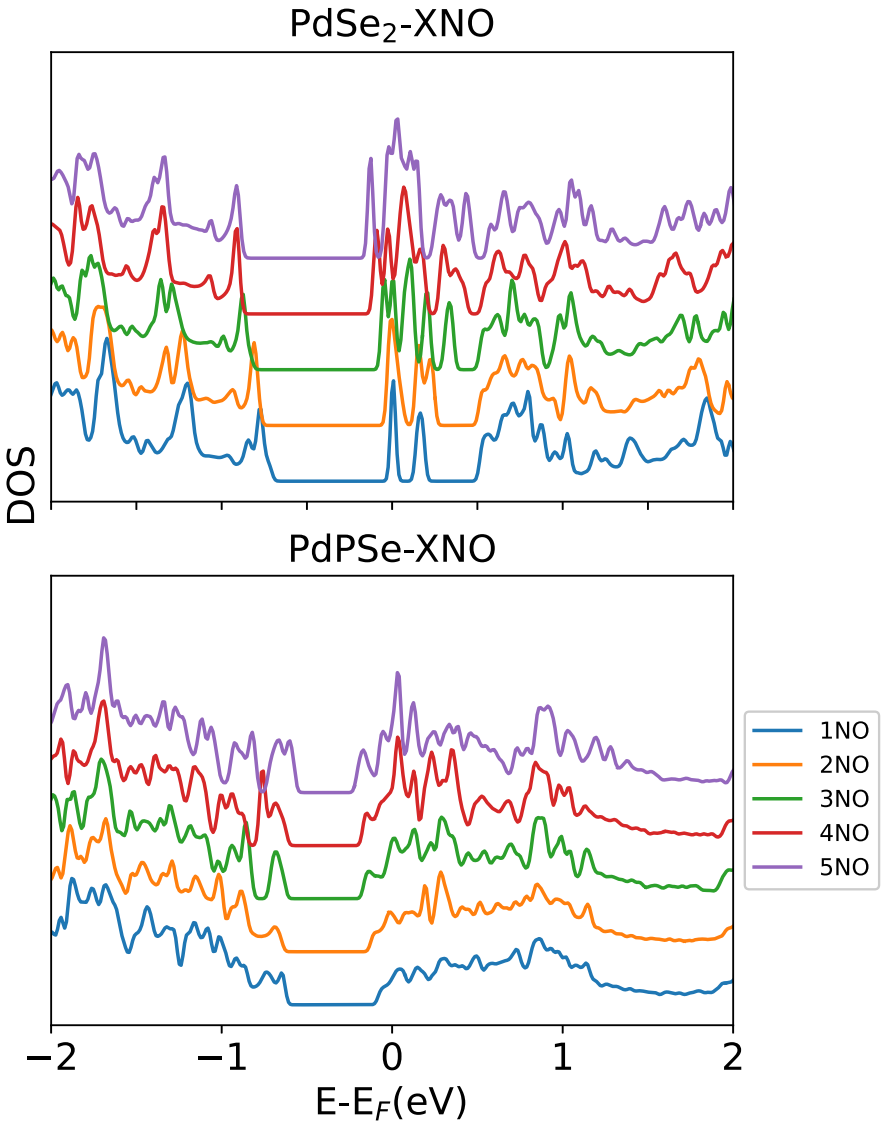

Figure 7: Total density of states for NO molecule adsorbed on penta-$PdSe_2$ and penta-PdPSe. Different concentrations of molecules are considered. Filled blue line: pristine monolayers.

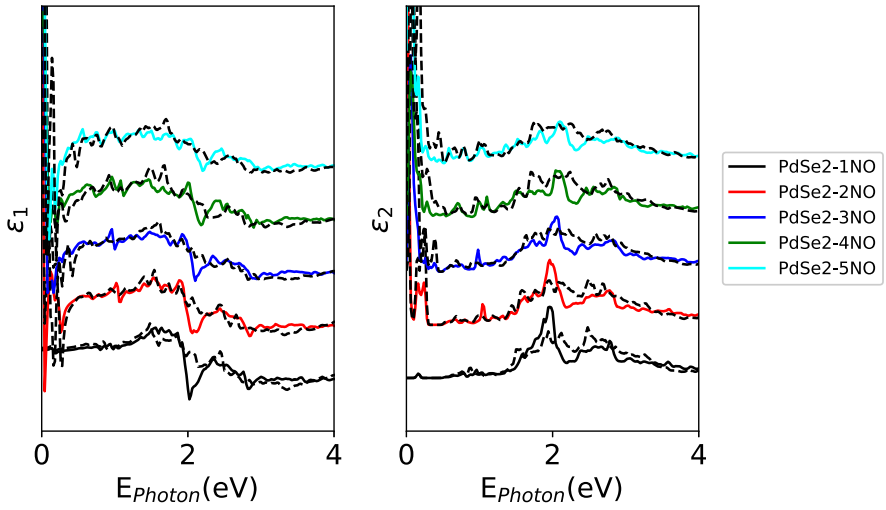

Figure 8: Dielectric function of NO molecules adsorbed on $PdSe_2$. Several concentrations of NO molecules are considered. Color lines are for light polarization in the x direction, and black dashed lines are for light polarization in the y direction.

function for both surfaces is anisotropic, with clearly different peak structures for each polarization of the incident light. Also, the shape of the dielectric function is affected by the increase in the concentration of NO molecules. This effect is especially observed in the infrared region and around a photon energy of 2 eV. Changes in the refractive index can be the basis for low-cost optical gas sensors, [49], so we report this variation of magnitude for penta-Pd surfaces upon the adsorption of NO molecules, considering different polarizations of the incident light and concentrations of the adsorbed molecule.

The refractive index can be obtained from the dielectric function as:

$$n = \frac{\sqrt{\sqrt{\epsilon_1^2 + \epsilon_2^2} + \epsilon_1}}{\sqrt{2}} \tag{3}$$

where ϵ_1 and ϵ_2 are the real and imaginary parts of the dielectric function. We define the change in the refractive index as:

$$\Delta n = n_{penta-Pd} - n_{penta-Pd+XNO} \tag{4}$$

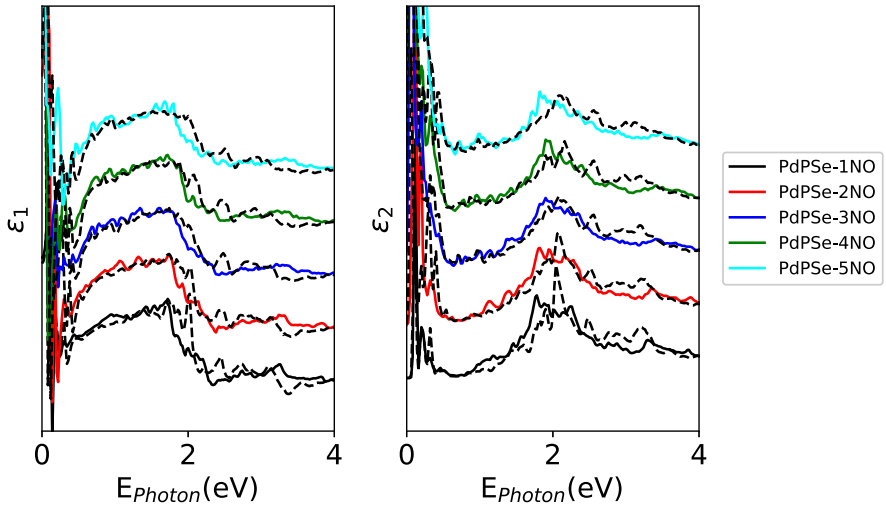

Figure 9: Dielectric function of NO molecules adsorbed on PdPSe. Several concentrations of NO molecules are considered. Color lines are for light polarization in the x direction, and black dashed lines are for light polarization in the y direction.

with $n_{penta-Pd}$ the refractive index of the surface and $n_{penta-Pd+XNO}$ the refractive index of the surface plus molecules, and X represents the number of NO molecules in the supercell. The results are shown in Figs 10 and 11. Each line represents a different NO concentration. They are vertically shifted to clarify the observation, and x and y polarization of the incident light are considered. Similar to the previous discussion about the dielectric function, the refractive index significantly changes in the infrared region and around a photon energy of 2 eV (details of these regions are shown in the Supplementary Material). The changes induced in the refraction index (Δn) are presented in Fig. 12 as a function of the NO concentration and polarization of the incident light for both penta-Pd surfaces. As previously, two linear polarizations, x and y, are considered. Negative values of Δn indicate an increase in the refractive index; using the information provided by Fig. 12, we have chosen a wavelength of 588 nm because of the substantial and systematic changes in the optical response for this value. Specifically, we have observed a quasi-linear increase of the refractive index with the NO concentration for the x-polarization of the incident light, with penta-$PdSe_2$ standing out. These changes in the refractive

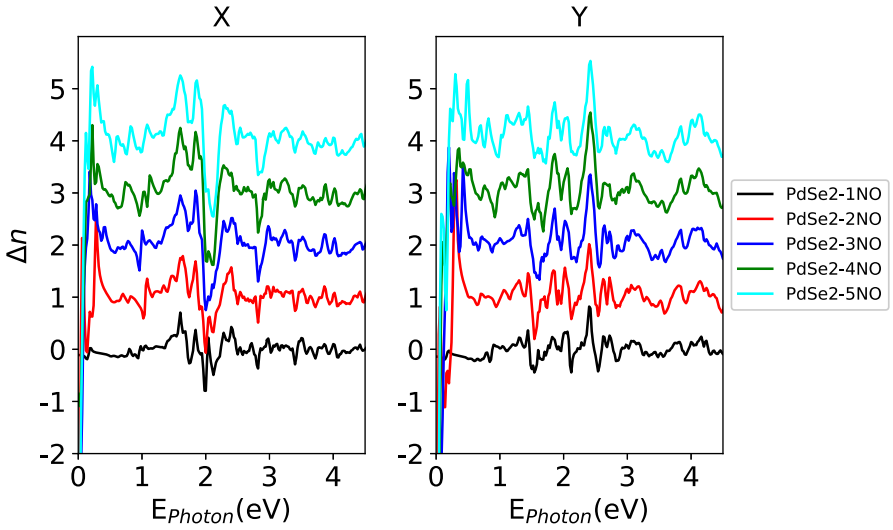

Figure 10: Change of the refractive indices of NO molecules adsorbed on $PdSe_2$ as a function of the photon energy. Several concentrations of NO molecules are considered. Two polarizations of the incident light are considered x and y directions.

index depend on the wavelength of the incident light and can be effectively utilized in developing fiber optical gas sensors, similar to those previously reported. In fact, a MoS_2/graphene composite was employed in a fiber-optic NO_2 gas sensor to enhance its selectivity [50].

4. Summary and Conclusions

In summary, we have calculated the electronic and optical properties of small molecules (H_2, CO, and NO) adsorbed on several positions of penta-$PdSe_2$ and penta-PdPSe. We have performed a systematic study combining several exchange-correlation functionals with two different representations of Kohn-Sham states. Our results suggest that all exchange-correlation functionals employed provide an adequate description of the geometric and electronic structure of penta-Pd materials. Therefore, for the choice of the specific functional computational time is a determinant factor. When small molecules are adsorbed onto the surfaces of penta-Pd, the opto-electronic responses of these surfaces change depending on the type of molecule, its position, and the surface. For H_2 and CO

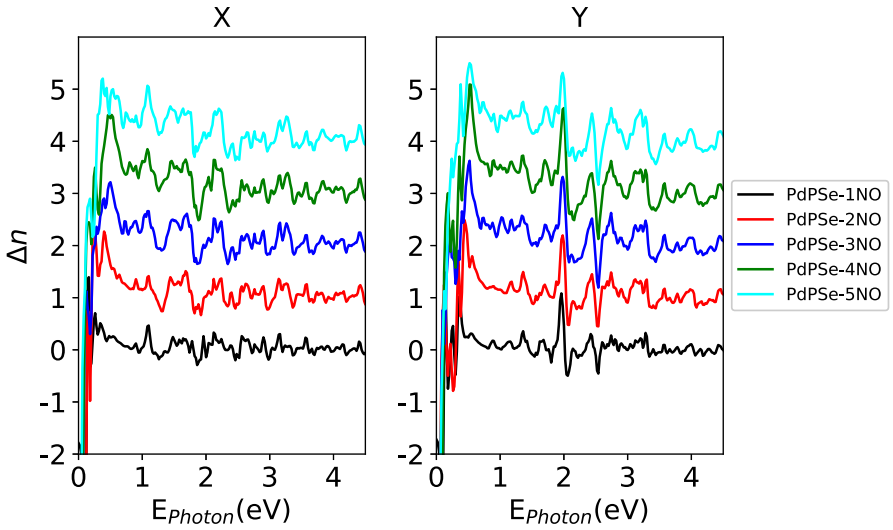

Figure 11: Change of the refractive indices of NO molecules adsorbed on PdPSe as a function of the photon energy. Several concentrations of NO molecules are considered. Two polarizations of the incident light are considered x and y directions.

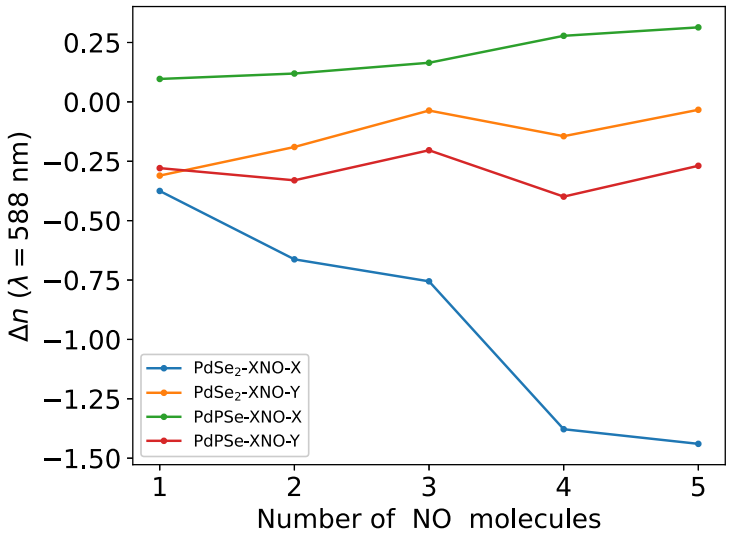

Figure 12: Change of the refractive indices of NO molecules adsorbed on penta-Pd surfaces as a function of the number of NO molecules adsorbed in the supercell. Two linear polarizations of the incident light are considered in the x and y directions.

molecules, our results indicate that the adsorption is weak and the electronic structure modification is too small to use these surfaces as sensors. However, for the NO molecule, our results show that adsorption energy is sufficient for the molecule to be sensed by penta-Pd surfaces. This is corroborated by the estimate of the recovery time from dynamic transition theory. Additionally, the NO molecule induces significant changes in the electronic structure of the Pd penta-surfaces, producing states around the Fermi level that render the system metallic. This amounts to a dramatic change in the conductivity of the complex. Finally, we explore variations on the refractive index to evaluate the potential of penta-Pd materials as sensors of NO molecules. Our results show significant changes in the refractive index as a function of the frequency and the polarization of the incident light, pointing to the use of penta-Pd materials as the main component for optical NO sensors.

Acknowledgments

JDC thanks MINCIENCIAS, Colombia, for the financial support of this research under contract 120680864729, and the hospitality of the Universidad Santa Maria during a research visit. LC acknowledges financial support from the Agencia Estatal de Investigación of Spain under grant PID2022-136285NB-C31, and from grant (MAD2D-CM)–(UCM5), Recovery, Transformation and Resilience Plan, funded by the European Union - NextGenerationEU. MP acknowledges the financial support of Chilean FONDECYT by Grant 1211913.

References

[1] K. S. Novoselov, A. K. Geim, S. V. Morozov, D. Jiang, M. I. Katsnelson, I. V. Grigorieva, S. V. Dubonos, A. A. Firsov, Two-dimensional gas of massless dirac fermions in graphene, Nature 438 (7065) (2005) 197–200. doi:10.1038/nature04233.

[2] P. Miró, M. Audiffred, T. Heine, An atlas of two-dimensional materials, Chem. Soc. Rev. 43 (18) (2014) 6537–6554. doi:10.1039/C4CS00102H.

[3] S. Haastrup, M. Strange, M. Pandey, T. Deilmann, P. S. Schmidt, N. F. Hinsche, M. N. Gjerding, D. Torelli, P. M. Larsen, A. C. Riis-Jensen, J. Gath, K. W. Jacobsen, J. J. Mortensen, T. Olsen,

K. S. Thygesen, The Computational 2D Materials Database: high-throughput modeling and discovery of atomically thin crystals, 2D Materials 5 (4) (2018) 042002, publisher: IOP Publishing. doi:10.1088/2053-1583/aacfc1.

[4] J. Zhou, L. Shen, M. D. Costa, K. A. Persson, S. P. Ong, P. Huck, Y. Lu, X. Ma, Y. Chen, H. Tang, Y. P. Feng, 2DMatPedia, an open computational database of two-dimensional materials from top-down and bottom-up approaches, Scientific Data 6 (1) (2019) 86. doi:10.1038/s41597-019-0097-3.

[5] F. A. Rasmussen, K. S. Thygesen, Computational 2D Materials Database: Electronic Structure of Transition-Metal Dichalcogenides and Oxides, The Journal of Physical Chemistry C 119 (23) (2015) 13169–13183. doi:10.1021/acs.jpcc.5b02950.

[6] R. Mas-Ballesté, C. Gómez-Navarro, J. Gómez-Herrero, F. Zamora, 2D materials: to graphene and beyond, Nanoscale 3 (2011) 20–30. doi:10.1039/C0NR00323A.

[7] J. R. Schaibley, H. Yu, G. Clark, P. Rivera, J. S. Ross, K. L. Seyler, W. Yao, X. Xu, Valleytronics in 2D materials, Nature Reviews Materials 1 (11) (2016) 1–15. doi:10.1038/natrevmats.2016.55.

[8] B. Luo, G. Liu, L. Wang, Recent advances in 2D materials for photocatalysis, Nanoscale 8 (2016) 6904–6920. doi:10.1039/C6NR00546B.

[9] M. Donarelli, L. Ottaviano, 2D materials for gas sensing applications: A review on graphene oxide, moS2, WS2 and phosphorene, Sensors 18 (11) (2018). doi:10.3390/s18113638.

[10] C. Zhu, D. Du, Y. Lin, Graphene and graphene-like 2D materials for optical biosensing and bioimaging: a review, 2D Materials 2 (3) (2015) 032004. doi:10.1088/2053-1583/2/3/032004.

[11] C. Huo, Z. Yan, X. Song, H. Zeng, 2D materials via liquid exfoliation: a review on fabrication and applications, Science Bulletin 60 (23) (2015) 1994–2008. doi:10.1007/s11434-015-0936-3.

[12] D. Geng, H. Y. Yang, Recent Advances in Growth of Novel 2D Materials: Beyond Graphene and Transition Metal Dichalcogenides, Advanced Materials 30 (45) (2018) 1800865. doi:10.1002/adma.201800865.

[13] C.-P. Tang, S.-J. Xiong, W.-J. Shi, J. Cao, Two-dimensional pentagonal crystals and possible spin-polarized Dirac dispersion relations, Journal of Applied Physics 115 (11) (2014) 113702. doi:10.1063/1.4868679.

[14] S. Zhang, J. Zhou, Q. Wang, X. Chen, Y. Kawazoe, P. Jena, Penta-graphene: A new carbon allotrope, Proceedings of the National Academy of Sciences 112 (8) (2015) 2372–2377. doi:10.1073/pnas.1416591112.

[15] M.-Q. Cheng, Q. Chen, K. Yang, W.-Q. Huang, W.-Y. Hu, G.-F. Huang, Penta-Graphene as a Potential Gas Sensor for NOx Detection, Nanoscale Research Letters 14 (1) (2019) 306. doi:10.1186/s11671-019-3142-4.

[16] M. Wang, Z. Zhang, Y. Gong, S. Zhou, J. Wang, Z. Wang, S. Wei, W. Guo, X. Lu, Penta-graphene as a promising controllable CO2 capture and separation material in an electric field, Applied Surface

Science 502 (2020) 144067. doi:10.1016/j.apsusc.2019.144067.

[17] B. Xiao, Y.-c. Li, X.-f. Yu, J.-b. Cheng, Penta-graphene: A promising anode material as the Li/Na-Ion battery with both extremely high theoretical capacity and fast charge/discharge rate, ACS Applied Materials & Interfaces 8 (51) (2016) 35342–35352. doi:10.1021/acsami.6b12727.

[18] F. Q. Wang, J. Yu, Q. Wang, Y. Kawazoe, P. Jena, Lattice thermal conductivity of penta-graphene, Carbon 105 (2016) 424–429. doi:10.1016/j.carbon.2016.04.054.

[19] C.-P. Zhang, B. Li, Z.-G. Shao, First-principle investigation of CO and CO2 adsorption on Fe-doped penta-graphene, Applied Surface Science 469 (2019) 641–646. doi:10.1016/j.apsusc.2018.11.072.

[20] Y. Aierken, O. Leenaerts, F. M. Peeters, A first-principles study of stable few-layer penta-silicene, Physical Chemistry Chemical Physics 18 (27) (2016) 18486–18492, publisher: The Royal Society of Chemistry. doi:10.1039/C6CP03200A.

[21] S. Sun, F. Meng, Y. Xu, J. He, Y. Ni, H. Wang, Flexible, auxetic and strain-tunable two dimensional penta-X2C family as water splitting photocatalysts with high carrier mobility, Journal of Materials Chemistry A 7 (13) (2019) 7791–7799, publisher: The Royal Society of Chemistry. doi:10.1039/C8TA12405A.

[22] Z. Liu, H. Wang, J. Sun, R. Sun, Z. F. Wang, J. Yang, Penta-Pt2N4: an ideal two-dimensional material for nanoelectronics, Nanoscale 10 (34) (2018) 16169–16177, publisher: The Royal Society of Chemistry. doi:10.1039/C8NR05561K.

[23] Y. Qu, C. T. Kwok, Y. Shao, X. Shi, Y. Kawazoe, H. Pan, Pentagonal transition-metal (group X) chalcogenide monolayers: Intrinsic semiconductors for photocatalysis, International Journal of Hydrogen Energy 46 (14) (2021) 9371–9379. doi:10.1016/j.ijhydene.2020.12.085.

[24] A. D. Oyedele, S. Yang, L. Liang, A. A. Puretzky, K. Wang, J. Zhang, P. Yu, P. R. Pudasaini, A. W. Ghosh, Z. Liu, C. M. Rouleau, B. G. Sumpter, M. F. Chisholm, W. Zhou, P. D. Rack, D. B. Geohegan, K. Xiao, PdSe2 pentagonal Two-dimensional layers with high air stability for electronics, Journal of the American Chemical Society 139 (40) (2017) 14090–14097. doi:10.1021/jacs.7b04865.

[25] R. Duan, C. Zhu, Q. Zeng, X. Wang, Y. Gao, Y. Deng, Y. He, J. Yang, J. Zhou, M. Xu, Z. Liu, PdPSe: Component-Fusion-Based Topology Designer of Two-Dimensional Semiconductor, Advanced Functional Materials 31 (35) (2021) 2102943. doi:10.1002/adfm.202102943.

[26] Two-dimensional PdPS and PdPSe nanosheets: Novel promising sensing platforms for harmful gas molecules | Elsevier Enhanced Reader. doi:10.1016/j.apsusc.2021.152115.

[27] C. Long, Y. Liang, H. Jin, B. Huang, Y. Dai, PdSe2: Flexible Two-Dimensional Transition Metal Dichalcogenides Monolayer for Water Splitting Photocatalyst with Extremely Low Recombination Rate, ACS Applied Energy Materials 2 (1) (2019) 513–520, publisher: American Chemical Society. doi:10.1021/acsaem.8b01521.

[28] J. J. Mortensen, L. B. Hansen, K. W. Jacobsen, Real-space grid implementation of the projector

augmented wave method, Physical Review B 71 (3) (2005) 035109, publisher: American Physical Society. doi:10.1103/PhysRevB.71.035109.

[29] J. Enkovaara, C. Rostgaard, J. J. Mortensen, J. Chen, M. Dułak, L. Ferrighi, J. Gavnholt, C. Glinsvad, V. Haikola, H. A. Hansen, H. H. Kristoffersen, M. Kuisma, A. H. Larsen, L. Lehtovaara, M. Ljungberg, O. Lopez-Acevedo, P. G. Moses, J. Ojanen, T. Olsen, V. Petzold, N. A. Romero, J. Stausholm-Møller, M. Strange, G. A. Tritsaris, M. Vanin, M. Walter, B. Hammer, H. Häkkinen, G. K. H. Madsen, R. M. Nieminen, J. K. Nørskov, M. Puska, T. T. Rantala, J. Schiøtz, K. S. Thygesen, K. W. Jacobsen, Electronic structure calculations with GPAW: a real-space implementation of the projector augmented-wave method, Journal of Physics: Condensed Matter 22 (25) (2010) 253202. doi:10.1088/0953-8984/22/25/253202.

[30] J. M. Soler, E. Artacho, J. D. Gale, A. García, J. Junquera, P. Ordejón, D. Sánchez-Portal, The siesta method for ab initio order-n materials simulation, Journal of Physics: Condensed Matter 14 (11) (2002) 2745. doi:10.1088/0953-8984/14/11/302.

[31] J. P. Perdew, K. Burke, M. Ernzerhof, Generalized Gradient Approximation Made Simple, Physical Review Letters 77 (18) (1996) 3865–3868, publisher: American Physical Society. doi:10.1103/PhysRevLett.77.3865.

[32] B. Hammer, L. B. Hansen, J. K. Nørskov, Improved adsorption energetics within density-functional theory using revised perdew-burke-ernzerhof functionals, Phys. Rev. B 59 (1999) 7413–7421. doi:10.1103/PhysRevB.59.7413.

[33] Y. Zhang, W. Yang, Comment on "generalized gradient approximation made simple", Phys. Rev. Lett. 80 (1998) 890–890. doi:10.1103/PhysRevLett.80.890.

[34] K. Lee, E. D. Murray, L. Kong, B. I. Lundqvist, D. C. Langreth, Higher-accuracy van der Waals density functional, Physical Review B 82 (8) (2010) 081101, publisher: American Physical Society. doi:10.1103/PhysRevB.82.081101.

[35] J. Klimeš, D. R. Bowler, A. Michaelides, Chemical accuracy for the van der Waals density functional, Journal of Physics: Condensed Matter 22 (2) (2009) 022201, publisher: IOP Publishing. doi:10.1088/0953-8984/22/2/022201.

[36] P. Li, J. Zhang, C. Zhu, W. Shen, C. Hu, W. Fu, L. Yan, L. Zhou, L. Zheng, H. Lei, Z. Liu, W. Zhao, P. Gao, P. Yu, G. Yang, Penta-PdPSe: A new 2D pentagonal material with highly in-plane optical, electronic, and optoelectronic anisotropy, Advanced Materials 33 (35) (2021) 2102541. doi:10.1002/adma.202102541.

[37] Y.-H. Kim, Y. Zhao, A. Williamson, M. J. Heben, S. B. Zhang, Nondissociative adsorption of h_2 molecules in light-element-doped fullerenes, Phys. Rev. Lett. 96 (2006) 016102. doi:10.1103/PhysRevLett.96.016102.

[38] J. I. G. Enriquez, A. R. C. Villagracia, Hydrogen adsorption on pristine, defected, and 3d-block

transition metal-doped penta-graphene, International Journal of Hydrogen Energy 41 (28) (2016) 12157–12166. doi:10.1016/j.ijhydene.2016.06.035.

[39] L. Wang, W. Li, Y. Cai, P. Pan, J. Li, G. Bai, J. Xu, Characterization of Pt-or Pd-doped graphene based on density functional theory for H2 gas sensor, Materials Research Express 6 (9) (2019). doi:10.1088/2053-1591/ab2dc0.

[40] X. Zhang, R. Fang, D. Chen, G. Zhang, Using pd-doped γ-graphyne to detect dissolved gases in transformer oil: A density functional theory investigation, Nanomaterials 9 (10) (2019). doi:10.3390/nano9101490.

[41] J. Cheng, D. Hu, A. Yao, Y. Gao, H. Asadi, A computational study on the Pd-decorated ZnO nanocluster for H2 gas sensing: A comparison with experimental results, Physica E: Low-Dimensional Systems and Nanostructures 124 (June) (2020) 114237. doi:10.1016/j.physe.2020.114237.

[42] R. Krishnan, W.-S. Su, H.-T. Chen, A new carbon allotrope: Penta-graphene as a metal-free catalyst for co oxidation, Carbon 114 (2017) 465–472. doi:10.1016/j.carbon.2016.12.054.

[43] M. Q. Cheng, Q. Chen, K. Yang, W. Q. Huang, W. Y. Hu, G. F. Huang, Penta-Graphene as a Potential Gas Sensor for NOx Detection, Nanoscale Research Letters 14 (1) (2019). doi:10.1186/s11671-019-3142-4.

[44] A. Aasi, B. Mortazavi, B. Panchapakesan, Two-dimensional PdPS and PdPSe nanosheets: Novel promising sensing platforms for harmful gas molecules, Applied Surface Science 579 (2022) 152115. doi:10.1016/j.apsusc.2021.152115.

[45] M. Zhao, D. Zhang, S. Dong, A DFT study of NO2 and SO2 gas-sensing properties of InX (X = Cl, Br and I) monolayers, Journal of Materials Science 56 (2021) 11828–11837. doi:10.1007/s10853-021-06047-1.

[46] T. Y. Mi, D. M. Triet, N. T. Tien, Adsorption of gas molecules on penta-graphene nanoribbon and its implication for nanoscale gas sensor, Physics Open 2 (2020) 100014. doi:10.1016/j.physo.2020.100014.

[47] J. Zhao, A. Buldum, J. Han, J. P. Lu, Gas molecule adsorption in carbon nanotubes and nanotube bundles, Nanotechnology 13 (2) (2002) 195. doi:10.1088/0957-4484/13/2/312.

[48] P. Fuentealba, E. Chamorro, J. C. Santos, Chapter 5 understanding and using the electron localization function, in: A. Toro-Labbé (Ed.), Theoretical Aspects of Chemical Reactivity, Vol. 19 of Theoretical and Computational Chemistry, Elsevier, 2007, pp. 57–85. doi:10.1016/S1380-7323(07)80006-9.

[49] J. Villatoro, D. Monzón-Hernández, Low-cost optical fiber refractive-index sensor based on core diameter mismatch, Journal of lightwave technology 24 (3) (2006) 1409.

[50] M. Sangeetha, D. Madhan, Ultra sensitive molybdenum disulfide (MoS2)/graphene based hybrid

sensor for the detection of NO2 and formaldehyde gases by fiber optic clad modified method, Optics & Laser Technology 127 (2020) 106193. doi:10.1016/j.optlastec.2020.106193.